

Pressure-Induced Phase Transition and Band Gap Engineering in Propylammonium Lead Bromide Perovskite

Xiangting Ren,^{†,‡} Xiaozhi Yan,^{†,‡,‡,‡} Azkar Saeed Ahmad,[†] Hu Cheng,[†] Yanchun Li,[§] Yusheng Zhao,^{†,‡} Lin Wang,^{*,||} and Shanmin Wang^{*,†,||}

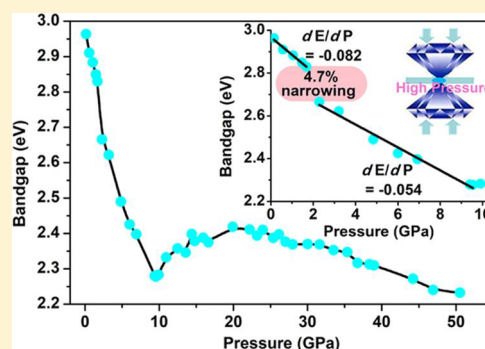
HPSTAR
786-2019

[†]Department of Physics and [‡]SUSTech Academy for Advanced Interdisciplinary Studies, Southern University of Science and Technology (SUSTech), Shenzhen, Guangdong 518055, P. R. China

[§]Beijing Synchrotron Radiation Facility, Institute of High Energy Physics, Chinese Academy of Sciences, Beijing 100049, China

^{||}Center for High Pressure Science and Technology Advanced Research (HPSTAR), Shanghai 201203, China

ABSTRACT: Organometal halide perovskites offer tremendous potential in developing optoelectronic and photovoltaic devices because of their spectacular band gap properties. Pressure has been demonstrated to be able to modulate their band gap in the energy range of visible spectrum, except in the high-energy region of ~ 2.5 – 3.0 eV. In this work, we present a high-pressure study of propylammonium lead bromide perovskite and reveal that the band gap can be tuned between the energy of violet light and yellow light (~ 3.0 – 2.2 eV) by pressure. Upon compression, the band gap of this material is progressively altered from ~ 3.0 eV at ambient pressure to 2.28 eV at 9.5 GPa. At a relatively low pressure of 1.3 GPa, a triclinic-to-monoclinic structural transition is also observed with a $\sim 4.7\%$ band gap reduction. Interestingly, in the pressure range of 9.5–20 GPa, the amorphization of the material leads to an anomalously enlarged band gap as a result of the disorder of organic cations, the slightly distorted $[\text{PbBr}_6]^{4-}$ octahedra. The variation of band gap of this perovskite at high pressures is explored to be closely attributed to the lattice density and octahedra distortion of amorphous phase. Findings of this work demonstrate that the band gap of organometal perovskites realizes the first redshift from the violet to visible region through the control of lattice parameter and crystal symmetry at high pressures, providing potential communication and sensing devices ranging from violet to yellow at high pressures. Our results also improve the understanding of the structures and properties of organometal halide perovskites.



1. INTRODUCTION

Organometal perovskites are a class of important semiconductors and have been extensively studied and used for a wide range of applications,¹ including solar cells,² photo-detectors,³ light-emitting diodes,⁴ and lasers,⁵ owing to their unique properties,⁶ such as tunable band gap,⁷ high absorption efficiency,⁸ and long charge diffusion distances.^{9,10} Most of these compounds preferably adopt perovskite-type crystal structures composed of an inorganic framework and organic anions with a general formula of ABX_3 , where A is an organic ammonium cation, B denotes Pb^{2+} or Sn^{2+} , and X represents the halide anion.¹¹ As commonly accepted, the electronic structure of organometal perovskites is mainly determined by the inorganic component, which strongly interacts with their surrounded organic anions.^{12–15} As a result, the electronic properties such as the mobility of charge carrier^{10,16–19} and band gap^{7,20–23} of these materials can easily be tuned by chemical methods (i.e., chemical pressure) by substitution of the metal cations, organic cations, or halide anions or by heteroelemental doping. However, the interaction between the organic and inorganic components is complicated and has not yet been well understood, but it is vital for understanding the

fundamental properties of these perovskites, calling for more rigorous data to explore this intriguing issue.

Alternative to chemical manipulation, pressure (P) provides a clean and effective approach to effectively tune the crystal structure and electronic properties without involving composition change. Because most organometal perovskites are very soft and compressible, their structural and electronic properties would be readily altered at high pressures.^{24–32} Decades of experimental efforts along this line have led to the discovery of a surge of new perovskite phases with exceptional electronic properties. Resistivity of MAPbBr_3 ($\text{MA} = \text{CH}_3\text{NH}_3^+$), for example, has been reported to show a significant increase by 5 orders of magnitude at high pressures, whereas its semiconducting character is well preserved.³³ In contrast, pressure-induced metallization in $(\text{MA})\text{PbI}_3$ semiconductor has recently been unveiled at 60 GPa.³⁴ A piezochromism phenomenon has also been observed in FAPbBr_3 (FA denotes $\text{NH}_2\text{CH}=\text{NH}_2^+$) at high pressures.³² However, to date, the study of organometal perovskites at high pressures is not sufficient and is limited to a

Received: March 26, 2019

Revised: May 24, 2019

Published: May 29, 2019

few material systems only, mainly including the methylammonium- and formamidinium-based halide perovskites. Moreover, the band gap in the region of ~ 2.5 – 3.0 eV has not been realized under pressure,³⁵ which is crucial for applications in optoelectronic and photovoltaic devices.

Among the organometal perovskites, propylammonium lead bromide, $\text{CH}_3\text{CH}_2\text{CH}_2\text{NH}_3\text{PbBr}_3$ (PAPbBr₃), is one of most exciting one-dimensional chain structure materials. This compound possesses a wide band gap of ~ 3.0 eV and is visibly transparent, holding great promise for wide variety of applications, such as transparent optoelectronics, fire and missile plume detections, and in devices for optical communications.^{36,37} The suitable structure and optimal band gap of PAPbBr₃ are key factors for these applications. However, PAPbBr₃ has sparsely been studied by far and the knowledge on the relationship between its structure and properties is still lacking, which will severely limit the fundamental study and practical applications of this material. In this work, we have systematically investigated the structural stability and optical properties of PAPbBr₃ using high-pressure X-ray diffraction and Raman, ultraviolet–visible (UV–vis) absorption, and photoluminescence spectroscopy measurements. Our experiments have led to a series of new discoveries for this material including pressure-induced structural transitions, amorphization, and band gap evolution, which will offer new opportunities for the study and application of organometal perovskites.

2. EXPERIMENTAL DETAILS

High-purity PAPbBr₃ microplates with an average thickness of $15\ \mu\text{m}$ and white color (>99% pure) were purchased from Xi'an Polymer Light Technology Corp. In situ high-pressure photoluminescence (PL) and Raman spectroscopy measurements were conducted using a Renishaw inVia Raman system equipped with two available excitation lasers of 325 and 532 nm in wavelength. The in situ high-pressure ultraviolet–visible (UV–vis) absorption spectroscopy experiment was performed using a deuterium–halogen light source, and the absorption data were collected using an optical fiber spectrometer with a response time of 1 s. The band gap of PAPbBr₃ was estimated by intercept of the absorption edge onto the energy axis from a plot $(ah\nu)^2$ versus photon energy ($h\nu$).³⁸ In situ high-pressure X-ray diffraction (XRD) experiments were performed at the 4W2 station of the Beijing Synchrotron Radiation facility (BSRF) with a wavelength of $0.6199\ \text{\AA}$. The collected two-dimensional (2D) diffraction patterns were integrated into one-dimensional spectra using the FIT2D program.³⁹ The XRD data were analyzed using the Pawley method.^{40,41} In each high-pressure experiment, a symmetrical diamond anvil cell (DAC) with a $300\ \mu\text{m}$ culet size was used to generate high pressures. A stainless steel T301 gasket was preindented to $\sim 40\ \mu\text{m}$ in thickness, and a sample hole of $120\ \mu\text{m}$ in diameter was drilled in the center of gasket. Before the experiment, the sample powders were loaded in the sample hole with silicon oil as the pressure-transmitting medium for improving hydrostatic pressure conditions. The pressure of the cell was calculated using a ruby scale.⁴² In fact, the material is soft enough and it can be served as a good pressure-transmitting medium for itself. Therefore, to maintain a clean sample environment, no pressure-transmitting medium was used for Raman, photoluminescence (PL), and XRD experiments.

3. RESULTS AND DISCUSSION

Figure 1a shows the integrated XRD patterns of PAPbBr₃ collected during compression and decompression at room

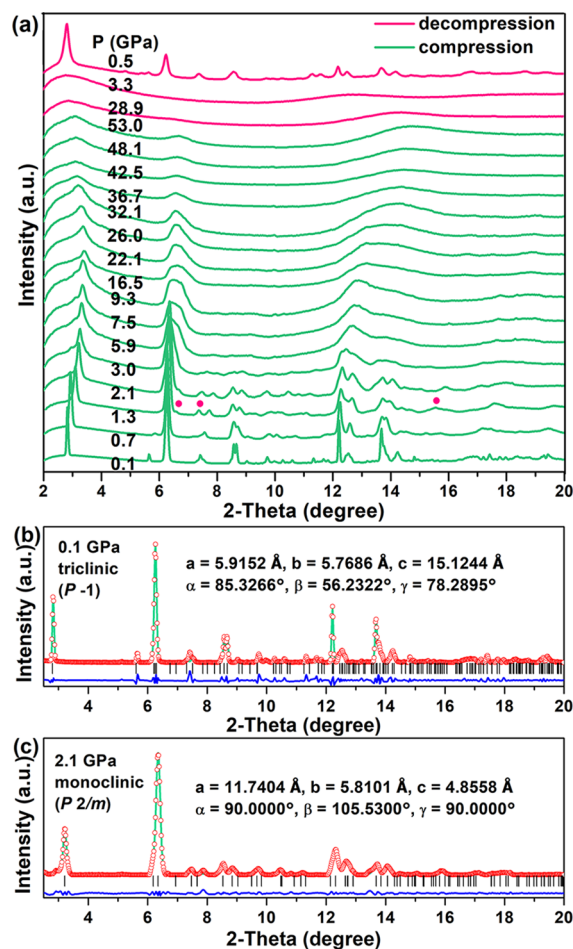


Figure 1. (a) Representative X-ray diffraction patterns of PAPbBr₃ taken during the compression and decompression processes at room temperature. (b–c) Refined XRD patterns taken at 0.1 and 2.1 GPa, respectively.

temperature. At low pressures, the XRD pattern can be indexed by a triclinic symmetry with space group $P\bar{1}$ (No. 2). For the XRD data taken at 0.1 GPa, the refined lattice parameters are $a = 5.9152\ \text{\AA}$, $b = 5.7686\ \text{\AA}$, and $c = 15.1244\ \text{\AA}$ (Figure 1b). With the increasing pressure, all Bragg diffraction peaks shift to the larger 2θ angle and are slightly broadened. Apparently, no phase transition is observed below 0.7 GPa. Above 1.3 GPa, a number of new weak peaks appear at 6.6 – 15.5° , indicating the occurrence of structure transformation. The new phase can be indexed by a $P2/m$ monoclinic phase with refined lattice parameters $a = 11.7404\ \text{\AA}$, $b = 5.8101\ \text{\AA}$, and $c = 4.8558\ \text{\AA}$ (Figure 1c). Above 9.3 GPa, a number of Bragg reflections disappear and leave behind a few profoundly broadened peaks, signaling the amorphization process with a significantly disordered structure. Because the chemical bonds in inorganic skeleton are much stronger than those in organic molecules, it is expected that the pressure would induce large disorder and distortion in the organic cation and the inorganic octahedra of PAPbBr₃, respectively. Because of the reversibility of phase transition, the amorphous phase starts to transform back to the $P\bar{1}$ phase below 3.3 GPa upon decompression and is

completely recovered at 0.5 GPa. A similar phenomenon has also been observed in other organic perovskite material systems.^{24,32,33}

To deeply understand the behavior of the organic cations at pressures, we performed high-pressure Raman spectroscopy measurement for PAPbBr₃, as shown in Figure 2. As the

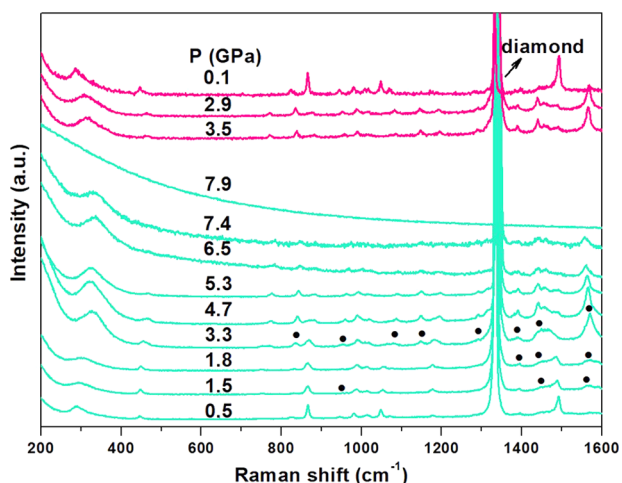


Figure 2. Raman spectra of PAPbBr₃ collected at different pressures and room temperatures. The strongest peak centered at 1333 cm⁻¹ corresponds to diamond. Green and pink lines denote the associated data taken on compression and decompression, respectively. The black solid dots represent new peaks at high pressures.

pressure is increased to 1.5 GPa, three new weak peaks appear in the Raman spectra and their intensities gradually increase with the increasing pressure. At 3.3 GPa, a few extra peaks suddenly emerge in the 800–1300 cm⁻¹ frequency range, corresponding to the triclinic–monoclinic phase transition as identified in the XRD experiment. At 7.9 GPa, the absence of Raman modes associated with the organic component suggests that the organic cations are severely disordered at high pressures. This is because the PA⁺ cation is very soft and its local structure is sensitive to pressure. The resultant pressure-induced amorphization is analogous to previous studies in other halide perovskites,³² owing to the disorder of organic cations and the tilting distortion of [PbBr₆]⁴⁻ octahedra. Additional atomic disorder of the interstitial organic molecules originates from shrinking of the disordered octahedral voids at pressures, which contributes to the amorphization process. With the decreasing pressure, such a high-pressure amorphous phase gradually recrystallizes back to its original structure (see Figure 2), which is in an excellent agreement with the XRD measurement.

Figure 3 shows the high-pressure PL spectra for PAPbBr₃. At ambient pressure, the sample has a strong emission band centered at ~409 nm, corresponding to the violet color in the visible spectrum range. Clearly, with the increasing pressure, the emission band is progressively shifted to the low-energy side of the spectrum, an indication of redshift. At ~1.3 GPa, two new peaks appear at around 430 and 480 nm, which confirm the structural transition in this compound as demonstrated in both XRD and Raman measurements. The observation of new PL peaks attributable to the P2/m polymorph suggests that the band gap is strongly affected by the pressure-induced reorientation of the [PbBr₆]⁴⁻ octahedral, and this phenomenon is similar to high-pressure PL spectra of

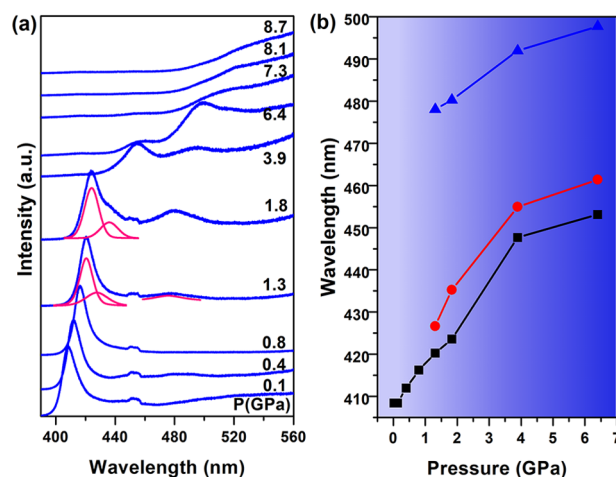


Figure 3. (a) Selected high-pressure PL spectra of PAPbBr₃ and (b) wavelength of the PL peak as a function of pressure.

FAPbI₃.⁴³ With further increasing the pressure, the intensity of the PL spectrum is rapidly reduced and almost undetectable above 7.3 GPa, likely due to the increased background and atomic disorder. The novel pressure dependence of the PL spectrum is similar to the situation in recently reported MAPbBr₃³³ and FAPbBr₃.³²

To determine the band gap, the UV–vis absorption spectroscopy measurement for this compound was performed at high pressures, as shown in Figure 4. The absorption edge

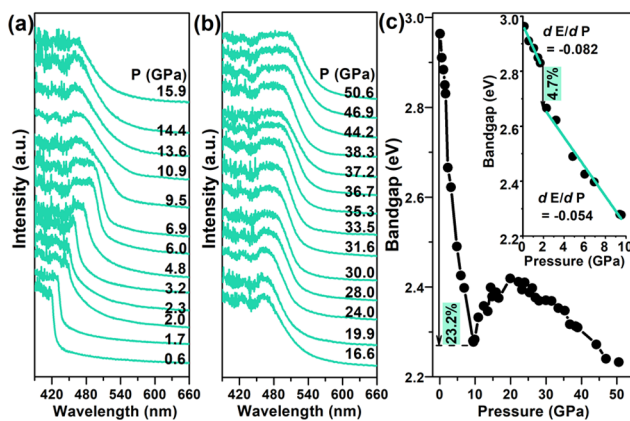


Figure 4. (a, b) Selected UV–vis absorption spectra of PAPbBr₃ under compression and (c) evolution of the band gap with pressure. The error bars are within the symbols. The inset is an enlarged portion to show details. The derived slopes are also included.

shows a gradual redshift as the pressure increases to ~9.5 GPa. Strikingly, a blueshift occurs in the pressure range of 10–20 GPa, followed by another redshift at pressure up to 50.6 GPa. For the lead bromide perovskites, band gaps are mainly attributed to the hybridized Pb 6s and Br 4p orbitals in the valence band and the Pb 6p orbital in the conduction band. Thus, the distortion of organic cations will influence the inorganic component, which is eventually manifested by the variation of band gap.^{13–15} As plotted in Figure 4c, the pressure dependence of band gap is determined using the Tauc method; at ambient conditions, the thus-determined band gap is 2.97 eV. Below 9.5 GPa, the reduction of band gap is a result of lattice contraction because the orbital will be largely overlapped and will consequently increase the band dispersion

as the bond is shortened at pressure. An abrupt decrease of band gap takes place at 1.7 GPa with a distinct slope change, inferring the occurrence of phase transition (inset of Figure 4c), in consistence with the observations in our XRD, Raman, and PL experiments. The slight differences of the phase transition pressure observed in the absorption, XRD, Raman, and PL measurements are possibly due to the different deviatoric stresses^{44,45} generated in DAC. It is noted that a 23.2% band gap narrowing is achieved at 9.5 GPa (i.e., $E_g \approx 2.28$ eV). Besides, the band structure of this material can be inferred from the shape of the absorption edge. At the critical pressure of 9.5 GPa, the absorption edge exhibits a dramatical shape change with a relatively flattened slope, implying a direct-to-indirect band gap transition. The blueshift of band gap in the pressure range of 10–20 GPa is mainly attributed to the pressure-induced amorphization because the overlap of elemental orbital is suppressed by the breaking of long-range order of atoms and the distortion of octahedra.³³ Apparently, pressure and amorphization have opposite effects on band gap and the latter trends to increase the band gap, in strikingly contrary to the former. From this point of view, the slight increase of band gap in the pressure range of 10–20 GPa can be more suitably explained as a result of the competition between two opposite effects at pressure and the amorphization effect prevails. This amorphization process is complete at 20 GPa and will not have a drastic influence on the band gap at higher pressures. Therefore, a decrease of band gap above 20 GPa should be intimately attributed to the pressure effect.

4. CONCLUSIONS

In summary, we have investigated the structural and electronic properties of PAPbBr₃ under high pressures. A pressure-induced triclinic-to-monoclinic phase transition and subsequent amorphization are observed. The pressure-induced amorphization is attributed to the destruction of long-range order of organic molecules and distortion of the Pb–Br skeleton. The large variation in band gap under pressure is observed and is found to be well correlated with the pressure-induced phase transition. Discoveries of this work provide an in-depth understanding of the variation of band gap in PAPbBr₃ due to lattice contraction and structural change at high pressures. The sensitivity of band gap of this material to pressure would provide a rational design strategy for the fabrication of PAPbBr₃-based sensor/switcher devices.

AUTHOR INFORMATION

Corresponding Authors

*E-mails: wanglin@hpstar.ac.cn (L.W.).

*E-mails: wangsm@sustech.edu.cn (W.S.).

ORCID

Lin Wang: 0000-0003-2931-7629

Shanmin Wang: 0000-0001-7273-2786

Author Contributions

[†]X.R. and X.Y. contributed equally to this work.

Notes

The authors declare no competing financial interest.

ACKNOWLEDGMENTS

This work is supported by the Shenzhen Peacock Plan (No. KQTD2016053019134356), the Guangdong Innovative & Entrepreneurial Research Team Program (No. 2016ZT06C279), and the Shenzhen Development and Reform

Commission Foundation for Novel Nano-Material Sciences, and the Research Platform for Crystal Growth & Thin-Film Preparation at SUSTech. We gratefully acknowledge the support of the National Natural Science Foundation of China (Grant no. 11704014 and 11874076) and the “Science Challenging Program (Grant No. JCKY2016212A501)”. The X-ray diffraction measurements were performed under Proposal no. 2018-BEPC-PT-001912 at the 4W2 station, Beijing Synchrotron Radiation Facility (BSRF) in China.

REFERENCES

- (1) Zhao, Y.; Zhu, K. Organic-Inorganic Hybrid Lead Halide Perovskites for Optoelectronic and Electronic Applications. *Chem. Soc. Rev.* **2016**, *45*, 655–689.
- (2) Lee, M. M.; Teuscher, J.; Miyasaka, T.; Murakami, T. N.; Snaith, H. J. Efficient Hybrid Solar Cells Based on Meso-Superstructured Organometal Halide Perovskites. *Science* **2012**, *338*, 643–647.
- (3) Dou, L.; Yang, Y. M.; You, J.; Hong, Z.; Chang, W. H.; Li, G.; Yang, Y. Solution-Processed Hybrid Perovskite Photodetectors with High Detectivity. *Nat. Commun.* **2014**, *5*, No. 5404.
- (4) Kim, Y. H.; Cho, H.; Heo, J. H.; Kim, T. S.; Myoung, N. S.; Lee, C. L.; Im, S. H.; Lee, T. W. Multicolored Organic/Inorganic Hybrid Perovskite Light-Emitting Diodes. *Adv. Mater.* **2015**, *27*, 1248–1254.
- (5) Xing, G.; Mathews, N.; Lim, S. S.; Yantara, N.; Liu, X.; Sabba, D.; Grätzel, M.; Mhaisalkar, S.; Sum, T. C. Low-Temperature Solution-Processed Wavelength-Tunable Perovskites for Lasing. *Nat. Mater.* **2014**, *13*, 476–480.
- (6) Huang, J.; Yuan, Y.; Shao, Y.; Yan, Y. Understanding the Physical Properties of Hybrid Perovskites for Photovoltaic Applications. *Nat. Rev. Mater.* **2017**, *2*, No. 17042.
- (7) D’Innocenzo, V.; Srimath Kandada, A. R.; De Bastiani, M.; Gandini, M.; Petrozza, A. Tuning the Light Emission Properties by Band Gap Engineering in Hybrid Lead Halide Perovskite. *J. Am. Chem. Soc.* **2014**, *136*, 17730–17733.
- (8) De Wolf, S.; Holovsky, J.; Moon, S. J.; Löper, P.; Niesen, B.; Ledinsky, M.; Haug, F. J.; Yum, J. H.; Ballif, C. Organometallic Halide Perovskites: Sharp Optical Absorption Edge and Its Relation to Photovoltaic Performance. *J. Phys. Chem. Lett.* **2014**, *5*, 1035–1039.
- (9) Stranks, S. D.; Eperon, G. E.; Grancini, G.; Menelaou, C.; Alcocer, M. J. P.; Leijtens, T.; Herz, L. M.; Petrozza, A.; Snaith, H. J. Electron-Hole Diffusion Lengths Exceeding 1 Micrometer in an Organometal Trihalide Perovskite Absorber. *Science* **2013**, *342*, 341–344.
- (10) Wehrenfennig, C.; Eperon, G. E.; Johnston, M. B.; Snaith, H. J.; Herz, L. M. High Charge Carrier Mobilities and Lifetimes in Organolead Trihalide Perovskites. *Adv. Mater.* **2014**, *26*, 1584–1589.
- (11) Nagane, S.; Bansode, U.; Game, O.; Chhatre, S.; Ogale, S. CH₃NH₃PbI_(3-x)(BF₄)_x: Molecular Ion Substituted Hybrid Perovskite. *Chem. Commun.* **2014**, *50*, 9741–9744.
- (12) Brivio, F.; Walker, A. B.; Walsh, A. Structural and Electronic Properties of Hybrid Perovskites for High-Efficiency Thin-Film Photovoltaics from First-Principles. *APL Mater.* **2013**, *1*, No. 042111.
- (13) Smith, M. D.; Pedesseau, L.; Kepenekian, M.; Smith, I. C.; Katan, C.; Even, J.; Karunadasa, H. I. Decreasing the Electronic Confinement in Layered Perovskites through Intercalation. *Chem. Sci.* **2017**, *8*, 1960–1968.
- (14) Umebayashi, T.; Asai, K.; Kondo, T.; Nakao, A. Electronic Structures of Lead Iodide Based Low-Dimensional Crystals. *Phys. Rev. B* **2003**, *67*, No. 155405.
- (15) Im, J.; Stoumpos, C. C.; Jin, H.; Freeman, A. J.; Kanatzidis, M. G. Antagonism between Spin–Orbit Coupling and Steric Effects Causes Anomalous Band Gap Evolution in the Perovskite Photovoltaic Materials CH₃NH₃Sn_{1-x}Pb_xI₃. *J. Phys. Chem. Lett.* **2015**, *6*, 3503–3509.
- (16) Johnston, M. B.; Herz, L. M. Hybrid Perovskites for Photovoltaics: Charge-Carrier Recombination, Diffusion, and Radiative Efficiencies. *Acc. Chem. Res.* **2016**, *49*, 146–154.

- (17) Oga, H.; Saeki, A.; Ogomi, Y.; Hayase, S.; Seki, S. Improved Understanding of the Electronic and Energetic Landscapes of Perovskite Solar Cells: High Local Charge Carrier Mobility, Reduced Recombination, and Extremely Shallow Traps. *J. Am. Chem. Soc.* **2014**, *136*, 13818–13825.
- (18) Shi, D.; Adinolfi, V.; Comin, R.; Yuan, M.; Alarousu, E.; Buin, A.; Chen, Y.; Hoogland, S.; Rothenberger, A.; Katsiev, K.; et al. Low Trap-State Density and Long Carrier Diffusion in Organolead Trihalide Perovskite Single Crystals. *Science* **2015**, *347*, 519–522.
- (19) Ponceca, C. S.; Savenije, T. J.; Abdellah, M.; Zheng, K.; Yartsev, A.; Pascher, T.; Harlang, T.; Chabera, P.; Pullerits, T.; Stepanov, A.; et al. Organometal Halide Perovskite Solar Cell Materials Rationalized: Ultrafast Charge Generation, High and Microsecond-Long Balanced Mobilities, and Slow Recombination. *J. Am. Chem. Soc.* **2014**, *136*, 5189–5192.
- (20) Knutson, J. L.; Martin, J. D.; Mitzi, D. B. Tuning the Band Gap in Hybrid Tin Iodide Perovskite Semiconductors Using Structural Templating. *Inorg. Chem.* **2005**, *44*, 4699–4705.
- (21) Noh, J. H.; Im, S. H.; Heo, J. H.; Mandal, T. N.; Seok, S. Chemical Management for Colorful, Efficient, and Stable Inorganic-Organic Hybrid Nanostructured Solar Cells. *Nano Lett.* **2013**, *13*, 1764–1769.
- (22) Sourisseau, S.; Louvain, N.; Bi, W.; Mercier, N.; Rondeau, D.; Boucher, F.; Buzaré, J. Y.; Legein, C. Reduced Band Gap Hybrid Perovskites Resulting from Combined Hydrogen and Halogen Bonding at the Organic-Inorganic Interface. *Chem. Mater.* **2007**, *19*, 600–607.
- (23) Walsh, A. Principles of Chemical Bonding and Band Gap Engineering in Hybrid Organic-Inorganic Halide Perovskites. *J. Phys. Chem. C* **2015**, *119*, 5755–5760.
- (24) Lü, X.; Wang, Y.; Stoumpos, C. C.; Hu, Q.; Guo, X.; Chen, H.; Yang, L.; Smith, J. S.; Yang, W.; Zhao, Y.; et al. Enhanced Structural Stability and Photo Responsiveness of $\text{CH}_3\text{NH}_3\text{SnI}_3$ Perovskite via Pressure-Induced Amorphization and Recrystallization. *Adv. Mater.* **2016**, *28*, 8663–8668.
- (25) Jiang, S.; Fang, Y.; Li, R.; Xiao, H.; Crowley, J.; Wang, C.; White, T. J.; Goddard, W. A.; Wang, Z.; Baikie, T.; et al. Pressure-Dependent Polymorphism and Band-Gap Tuning of Methylammonium Lead Iodide Perovskite. *Angew. Chem., Int. Ed.* **2016**, *55*, 6540–6544.
- (26) Lü, X.; Yang, W.; Jia, Q.; Xu, H. Pressure-Induced Dramatic Changes in Organic-Inorganic Halide Perovskites. *Chem. Sci.* **2017**, *8*, 6764–6776.
- (27) Jiang, S.; Luan, Y.; Jang, J. I.; Baikie, T.; Huang, X.; Li, R.; Saouma, F. O.; Wang, Z.; White, T. J.; Fang, J. Phase Transitions of Formamidinium Lead Iodide Perovskite under Pressure. *J. Am. Chem. Soc.* **2018**, *140*, 13952–13957.
- (28) Yin, T.; Fang, Y.; Chong, W. K.; Ming, K. T.; Jiang, S.; Li, X.; Kuo, J. L.; Fang, J.; Sum, T. C.; White, T. J.; et al. High-Pressure-Induced Comminution and Recrystallization of $\text{CH}_3\text{NH}_3\text{PbBr}_3$ Nanocrystals as Large Thin Nanoplates. *Adv. Mater.* **2018**, *30*, No. 1705017.
- (29) Jaffe, A.; Lin, Y.; Beavers, C. M.; Voss, J.; Mao, W. L.; Karunadasa, H. I. High-Pressure Single-Crystal Structures of 3D Lead-Halide Hybrid Perovskites and Pressure Effects on Their Electronic and Optical Properties. *ACS Cent. Sci.* **2016**, *2*, 201–209.
- (30) Liu, G.; Gong, J.; Kong, L.; Schaller, R. D.; Hu, Q.; Liu, Z.; Yan, S.; Yang, W.; Stoumpos, C. C.; Kanatzidis, M. G.; et al. Isothermal Pressure-Derived Metastable States in 2D Hybrid Perovskites Showing Enduring Bandgap Narrowing. *Proc. Natl. Acad. Sci. U.S.A.* **2018**, *115*, No. 201809167.
- (31) Liu, G.; Kong, L.; Gong, J.; Yang, W.; Mao, H. K.; Hu, Q.; Liu, Z.; Schaller, R. D.; Zhang, D.; Xu, T. Pressure-Induced Bandgap Optimization in Lead-Based Perovskites with Prolonged Carrier Lifetime and Ambient Retainability. *Adv. Funct. Mater.* **2017**, *27*, No. 1604208.
- (32) Wang, L.; Wang, K.; Zou, B. Pressure-Induced Structural and Optical Properties of Organometal Halide Perovskite-Based Formamidinium Lead Bromide. *J. Phys. Chem. Lett.* **2016**, *7*, 2556–2562.
- (33) Wang, Y.; Lü, X.; Yang, W.; Wen, T.; Yang, L.; Ren, X.; Wang, L.; Lin, Z.; Zhao, Y. Pressure-Induced Phase Transformation, Reversible Amorphization, and Anomalous Visible Light Response in Organolead Bromide Perovskite. *J. Am. Chem. Soc.* **2015**, *137*, 11144–11149.
- (34) Jaffe, A.; Lin, Y.; Mao, W. L.; Karunadasa, H. I. Pressure-Induced Metallization of the Halide Perovskite $(\text{CH}_3\text{NH}_3)\text{PbI}_3$. *J. Am. Chem. Soc.* **2017**, *139*, 4330–4333.
- (35) Liu, G.; Kong, L.; Yang, W.; Mao, H. Pressure Engineering of Photovoltaic Perovskites. *Mater. Today* 2019, in press. DOI: 10.1016/j.mattod.2019.02.016.
- (36) Zhengyuan, X.; Brian, M. S. Ultraviolet Communications: Potential and State-of-the-Art. *IEEE Commun. Mag.* **2008**, *46*, 67–73.
- (37) Wager, J. F. Transparent Electronics. *Science* **2003**, *300*, 1245–1247.
- (38) Tauc, J. Optical Properties and Electronic Structure of Amorphous Ge and Si - ScienceDirect. *Mater. Res. Bull.* **1968**, *3*, 37–46.
- (39) Hammersley, A. P.; Svensson, S. O.; Hanfland, M.; Fitch, A. N.; Hausermann, D. Two-Dimensional Detector Software: From Real Detector to Idealised Image or Two-Theta Scan. *High Pressure Res.* **1996**, *14*, 235–248.
- (40) Rietveld, H. M. Line Profiles of Neutron Powder-Diffraction Peaks for Structure Refinement. *Acta Crystallogr.* **1967**, *22*, 151–152.
- (41) Chatterjee, A.; Bhat, A.; Matocha, K. Investigation of Electrically Active Defects of Silicon Carbide Using Atomistic Scale Modeling and Simulation. *Phys. B* **2007**, *401–402*, 81–84.
- (42) Mao, H. K.; Xu, J.; Bell, P. M. Calibration of the Ruby Pressure Gauge to 800 Kbar under Quasi-Hydrostatic Conditions. *J. Geophys. Res.* **1986**, *91*, 4673.
- (43) Jiang, S.; Luan, Y.; Jang, J. I.; Baikie, T.; Huang, X.; Li, R.; Saouma, F. O.; Wang, Z.; White, T. J.; Fang, J. Phase Transitions of Formamidinium Lead Iodide Perovskite under Pressure. *J. Am. Chem. Soc.* **2018**, *140*, 13952–13957.
- (44) Wang, Z.; Schliehe, C.; Wang, T.; Nagaoka, Y.; Cao, Y. C.; Bassett, W. A.; Wu, H.; Fan, H.; Weller, H. Deviatoric Stress Driven Formation of Large Single-Crystal PbS Nanosheet from Nanoparticles and in Situ Monitoring of Oriented Attachment. *J. Am. Chem. Soc.* **2011**, *133*, 14484–14487.
- (45) Wang, T.; Li, R.; Quan, Z.; Loc, W. S.; Bassett, W. A.; Xu, H.; Cao, Y. C.; Fang, J.; Wang, Z. Pressure Processing of Nanocube Assemblies Toward Harvesting of a Metastable PbS Phase. *Adv. Mater.* **2015**, *27*, 4544–4549.